Inactivation of Chibby affects function of motile airway cilia

Vera A. Voronina,[1,4,5] Ken-Ichi Takemaru,[7] Piper Treuting,[2] Damon Love,[7] Barbara R. Grubb,[6] Adeline M. Hajjar,[3] Allison Adams,[1,4,5] Feng-Qian Li,[7] and Randall T. Moon[1,4,5]

[1]Department of Pharmacology, [2]Department of Comparative Medicine, [3]Department of Immunology, [4]Howard Hughes Medical Institute, and [5]Institute for Stem Cell and Regenerative Medicine, University of Washington, Seattle, WA 98195
[6]Cystic Fibrosis Pulmonary Research and Treatment Center, Department of Medicine, University of North Carolina at Chapel Hill, Chapel Hill, NC 27599
[7]Department of Pharmacological Sciences, State University of New York at Stony Brook, Stony Brook, NY 11794

Chibby (Cby) is a conserved component of the Wnt–β-catenin pathway. Cby physically interacts with β-catenin to repress its activation of transcription. To elucidate the function of Cby in vertebrates, we generated $Cby^{-/-}$ mice and found that after 2–3 d of weight loss, the majority of mice die before or around weaning. All $Cby^{-/-}$ mice develop rhinitis and sinusitis. When challenged with *Pseudomonas aeruginosa* isolates, $Cby^{-/-}$ mice are unable to clear the bacteria from the nasal cavity. Notably, $Cby^{-/-}$ mice exhibit a complete absence of mucociliary transport caused by a marked paucity of motile cilia in the nasal epithelium. Moreover, ultrastructural experiments reveal impaired basal body docking to the apical surface of multiciliated cells. In support of these phenotypes, endogenous Cby protein is localized at the base of cilia. As the phenotypes of $Cby^{-/-}$ mice bear striking similarities to primary ciliary dyskinesia, $Cby^{-/-}$ mice may prove to be a useful model for this condition.

Introduction

Chibby (Cby) was originally discovered as an inhibitor of the Wnt–β-catenin pathway (Takemaru et al., 2003). Cby inhibits Wnt–β-catenin signaling through two distinct mechanisms: by competing with T cell factor/lymphoid-enhancer factor transcription factors for binding β-catenin (Takemaru et al., 2003) and by facilitating nuclear export of β-catenin (Li et al., 2008). Another study demonstrated that Cby also functions in the cytoplasm as a binding partner and a mediator of intracellular trafficking of Polycystin-2 (Hidaka et al., 2004), which is a protein required for the proper function of primary cilia (Nauli et al., 2003). Interestingly, Polycystin-2 is also found in the membrane of motile cilia, suggesting that it may be important for the function of this distinct subclass of cilia (Pazour et al., 2005; Teilmann et al., 2006; Christensen et al., 2007).

Cilia are eukaryotic organelles that are traditionally classified according to their microtubule composition, with the 9 + 0 arrangements in primary cilia and the 9 + 2 arrangements in motile cilia, although this classification is an oversimplification (Kramer-Zucker et al., 2005; Ong and Wagner, 2005; Davis et al., 2006). Primary cilia are present on most mammalian cells and play critical roles in mechanosensation, photoreception, olfaction, and intracellular signaling (Singla and Reiter, 2006). Motile cilia are less ubiquitous and are found primarily in epithelial cells lining the airways, reproductive tracts, and the ependyma and choroid plexus in the brain (Eley et al., 2005). They are important in clearing mucus and debris from the airway, circulating cerebrospinal fluid in the brain, and possibly transporting the cumulus–oocyte complex in the female reproductive tract (Salathe, 2007). Defects in motile cilia lead to a wide spectrum of phenotypes, including abnormal left–right patterning, infertility, hydrocephalus, and respiratory infections (Badano et al., 2006; Salathe, 2007). Various combinations of these phenotypes are present in multiple diseases, including primary ciliary dyskinesia (PCD; Badano et al., 2006).

The Rockefeller University Press $30.00
J. Cell Biol. Vol. 185 No. 2 225–233
www.jcb.org/cgi/doi/10.1083/jcb.200809144

JCB 225

THE JOURNAL OF CELL BIOLOGY

PCD, which includes Kartagener syndrome and the immotile cilia syndrome, is a rare genetically heterogeneous disorder with an estimated prevalence rate of 1 in 15,000 to 1 in 60,000, although the number of diagnosed cases is lower as a result of variability in symptoms and similarity to acquired conditions (Coren et al., 2002). The most common genetic causes of PCD are mutations in the human *DNAI1* and *DNAH5* genes, which encode outer dynein arm components (Pennarun et al., 1999; Olbrich et al., 2002). Mutations in these genes are responsible for up to 40% of the known cases of PCD (Zariwala et al., 2007). A small percentage of patients with PCD were reported to have mutations in *DNAH11*, *TXNDC3*, *RPGR*, or the *OFD1* gene, whereas other causative genes remain unidentified (Bush and Ferkol, 2006; Livraghi and Randell, 2007). Recurrent respiratory infections, chronic otitis media, and partially penetrant situs inversus are the hallmarks of PCD (Meeks and Bush, 2000). Mortality and morbidity associated with PCD are primarily caused by repeated infections resulting in respiratory insufficiency.

The lesions of PCD highlight the importance of efficient mucociliary clearance, which depends on mucus production and mucociliary transport (MCT). In the normal airway, goblet cells produce mucus that traps particles and pathogens. Coordinated ciliary beating transports mucus and embedded particles toward the larynx to be swallowed (Cohen, 2006). In patients with PCD, abnormal motility of airway cilia leads to an inability to transport mucus. Mucus plaques obstruct the airway and serve as a nidus for many opportunistic bacteria, including *Pseudomonas aeruginosa*.

In this study, we describe germline inactivation of the *Cby* gene and the resulting respiratory phenotype, which is similar to the clinical features observed in PCD patients. $Cby^{-/-}$ mice develop upper respiratory infections and are unable to clear bacteria because of the absence of MCT. We show that the MCT defects result, at least in part, from a marked paucity of motile cilia in the nasal epithelium possibly caused by the abnormal transport or docking of basal bodies to the apical membrane. In agreement with this phenotype, we demonstrate that Cby is normally localized at the base of the cilia in cultured MDCK2 cells and in nasal epithelial tissue. The perturbation of cilia and the corresponding effects on MCT render $Cby^{-/-}$ mice particularly suitable for studies of PCD and other chronic upper respiratory diseases.

Results and discussion

Cby expression

We first characterized the expression of mouse *Cby* in embryonic day (E) 9.5–11.5 embryos by whole mount in situ hybridization analysis using a probe specific for the *Cby* coding region. Our analysis showed that *Cby* is ubiquitously expressed at E9.5–11.5 (Fig. 1 A and not depicted). Northern blot analysis revealed that *Cby* is expressed in multiple adult tissues and throughout embryogenesis (Fig. 1 B and not depicted). These data establish a broad expression profile for *Cby* in the developing mouse embryo as well as the presence of *Cby* transcripts in multiple adult tissues.

Generation and initial characterization of $Cby^{-/-}$ mice

To investigate *Cby* function, we performed germline inactivation by removing the entire coding region of the mouse *Cby* gene (Fig. S1). We confirmed the loss of *Cby* RNA in knockout embryos by in situ hybridization using an antisense *Cby* probe. $Cby^{-/-}$ embryos lacked staining compared with heterozygous littermate controls (Fig. 1, compare A with C). $Cby^{-/-}$ embryos hybridized with the antisense probe were indistinguishable from control embryos stained with the sense probe (Fig. 1, compare C with D). Gross morphological evaluation of newborns did not reveal apparent defects. However, by 2 wk of age, $Cby^{-/-}$ pups were runted and demonstrated anemia, as indicated by decreased hematocrit on complete blood count analysis and reduced subcutaneous fat (Fig. 1 E and not depicted).

To better understand the association of *Cby* gene ablation with runting, we performed body mass and survival analysis of pups produced by $Cby^{+/-}$ parents. The survival analysis showed that $Cby^{-/-}$ mice stratified into two groups: the majority of them died by postnatal day (P) 25 (knockout-die), whereas a small percentage started to gain weight and survived for >18 mo (knockout-survive; Fig. 1, F and G). However, all surviving $Cby^{-/-}$ mice (7/32) continued to have low body mass compared with $Cby^{+/+}$ mice (Fig. 1 F). At all stages analyzed, $Cby^{+/-}$ mice were indistinguishable from $Cby^{+/+}$ counterparts (unpublished data). These data demonstrate that the gross physiological effect of loss of *Cby* on mouse development results in lowered body mass followed by early postnatal lethality. However, the exact causes of their postnatal death remain unknown.

Sinusitis and otitis in $Cby^{-/-}$ mice

Histopathological phenotyping demonstrated that all $Cby^{-/-}$ mice, both those that die postnatally and those that survive, develop sinusitis (Fig. 2, A and B). This presents itself as early as P7 and persists throughout the lifetime of the surviving adults. Mice with severe sinusitis also had otitis media (Fig. 2, C and D).

To further probe sinus function, we tested the susceptibility of $Cby^{-/-}$ mice to bacterial infection. We intranasally infected five $Cby^{-/-}$, five $Cby^{+/-}$, and six $Cby^{+/+}$ mice with *P. aeruginosa*, a pathogenic bacterium frequently associated with chronic airway infection in patients with cystic fibrosis (CF) and PCD (Gibson et al., 2003). We found that at 72 h after infection, infected littermate controls efficiently cleared bacteria and had no sinus inflammation, as revealed by histological analysis of the upper airways (Fig. 2 E). In contrast, all $Cby^{-/-}$ mice had accumulated abundant mucus and bacterial debris, leading to severe inflammation and distorted morphology of sinuses (Fig. 2 F). Concurrent colony-forming unit (CFU) analysis revealed that both $Cby^{-/-}$ and control mice successfully cleared the bacteria from the lungs (Fig. 2 G). Therefore, bacterial challenge revealed further phenotypic abnormalities, as $Cby^{-/-}$ mice develop sinus and middle ear inflammation and fail to clear bacteria from the sinuses.

Normal bioelectric and impaired MCT in $Cby^{-/-}$ mice

Defects in bacterial clearance can have multiple etiologies, as illustrated by PCD and CF. Although respiratory phenotypes
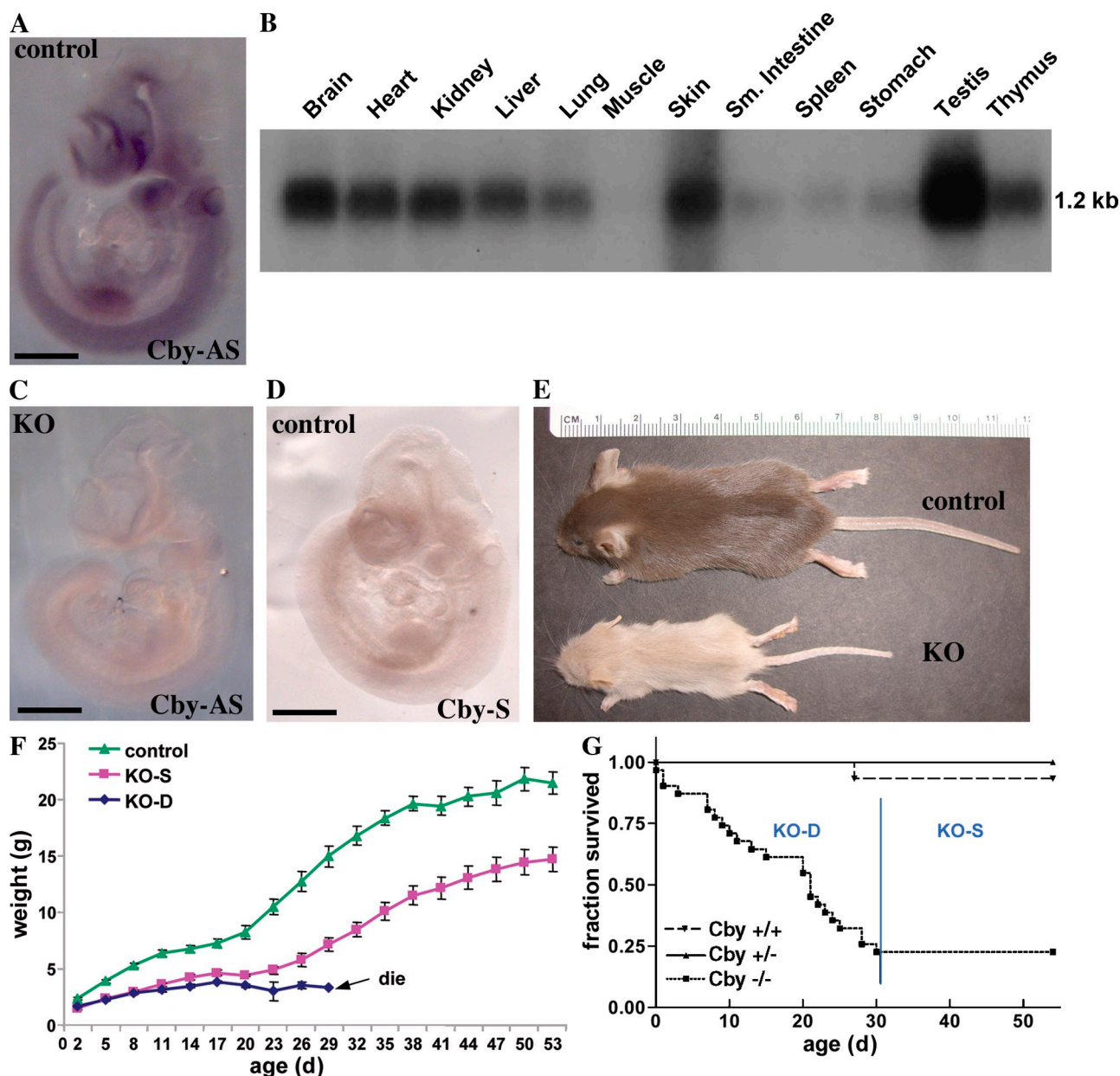
Figure 1. **Mouse *Cby* expression and a postnatal lethality of *Cby*$^{-/-}$ mice.** (A) *Cby*$^{+/+}$ E10.5 embryo hybridized with antisense (AS) *Cby* probe. (B) A single *Cby* transcript of 1.2 kb was detected by Northern blot analysis in the adult mouse tissues. (C) *Cby*$^{-/-}$ E10.5 embryo hybridized with antisense *Cby* probe. (D) *Cby*$^{+/+}$ E10.5 embryo hybridized with *Cby* sense (S) probe. (E) P20 *Cby*$^{+/+}$ and *Cby*$^{-/-}$ littermates. (F) Body weight analysis of *Cby*$^{-/-}$ and control mice on a regular chow diet. The control group included three males and three females, whereas the *Cby*$^{-/-}$ group had 28 animals at P2 that diminished to seven knockout-survive (KO-S) animals at the end of the study. Error bars represent SEM. (G) Kaplan-Meyer survival curves for *Cby*$^{+/+}$ (n = 15), *Cby*$^{+/-}$ (n = 23), and *Cby*$^{-/-}$ (n = 32) mice. KO, knockout; KO-D, knockout-die. Bars, 1 mm.

observed in PCD and CF patients are quite similar, the molecular and cellular mechanisms underlying these phenotypes differ. As previously mentioned, abnormal airway cilia structure or motility underlies PCD phenotypes (Livraghi and Randell, 2007). In contrast, human patients with CF caused by mutations in the CF transmembrane conductance regulator exhibit abnormal ion and water transport secondary to defects in Cl$^-$ conductance. This leads to depletion of the periciliary aqueous layer in the respiratory system with accumulation of abnormally viscous mucus that adheres to the epithelial surfaces and cannot be transported by cilia (Livraghi and Randell, 2007).

To address potential ion channel deficiencies in *Cby*$^{-/-}$ mice, we determined Na$^+$ absorption in response to amiloride and Cl$^-$ secretion in response to UTP and forskolin in tracheas from *Cby*$^{+/+}$ and *Cby*$^{-/-}$ mice. The tracheal bioelectrics were identical between the two genotypes (Fig. 2 H), indicating that ion channel function was not affected. These results argue against the involvement of ion channel defects in the airway pathology of *Cby*$^{-/-}$ mice.

Next, we examined ciliary function by measuring MCT in nasopharyngeal cavities. As expected, control mice exhibited normal MCT of endogenous particles in the nasal cavity. Strikingly,
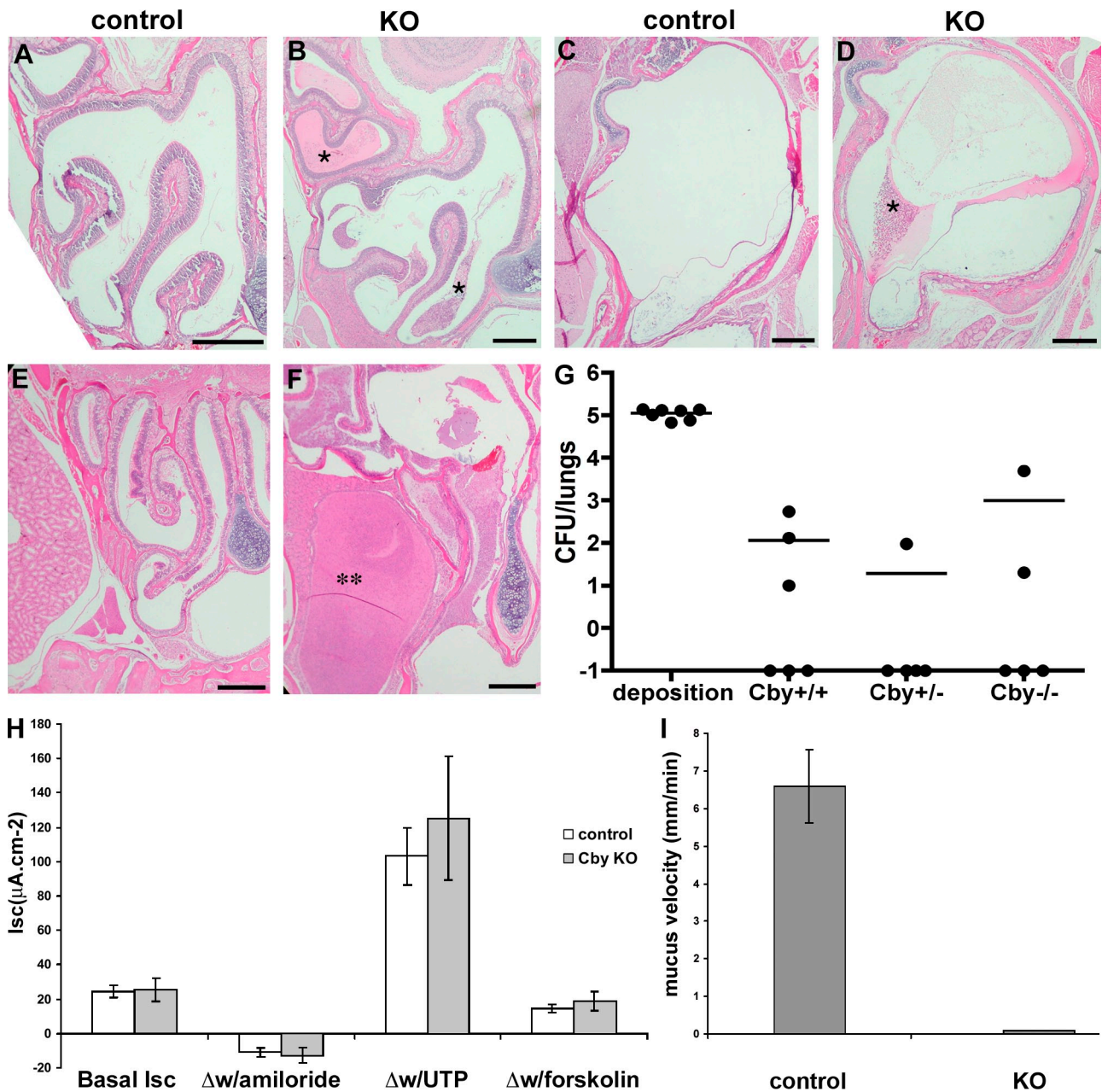
Figure 2. **Inflammation in sinuses and ears of Cby$^{-/-}$ mice.** (A and B) H&E staining of sinus sections from adult Cby$^{+/+}$ (A) and Cby$^{-/-}$ (B) mice. Asterisks label accumulation of protein-rich fluid. (C and D) H&E staining of middle ear sections from Cby$^{+/+}$ (C) and Cby$^{-/-}$ (D) mice. The asterisk indicates accumulation of inflammatory cells in protein-rich fluid. (E and F) H&E staining of sinus sections of the control (E) and Cby$^{-/-}$ (F) adult mice infected with *P. aeruginosa*. Upon intranasal infection, Cby$^{-/-}$ animals failed to clear bacteria and, at 72 h, developed a severe exudative sinusitis characterized by abundant accumulation of inflammatory cells and bacterial debris admixed in protein-rich fluid (asterisks). (G) Quantification of CFUs in the lungs of infected mice. A one-way analysis of variance test did not reveal a difference between three groups of mice (P = 0.6079). Results for individual mice are shown by dots and plotted on a log scale. Lines represent the mean number for each genotype. (H) Data shown are short circuit currents (Isc) or change in short circuit currents in response to amiloride, UTP, or forskolin added sequentially to the preparations. Open bars represent control tracheas (*n* = 6), and shaded bars represent Cby$^{-/-}$ tracheas (*n* = 4). Results are represented as means ± SEM. (I) MCT in the nasopharynx of adult control (*n* = 6) and Cby$^{-/-}$ (*n* = 4) mice. Data are represented as means ± SEM. KO, knockout. Bars, 500 µm.

the Cby$^{-/-}$ mice exhibited an MCT rate of 0 mm/min (Fig. 2 I). The cilia of the control mice generated a steady flow of mucus, whereas, in three of the four Cby$^{-/-}$ mice studied, mucus movements were completely absent (compare Video 1 with Video 2). In the fourth Cby$^{-/-}$ mouse, we observed small islands of local mucus movement, but this was not sufficient to generate detectable MCT. Thus, Cby$^{-/-}$ mice develop sinusitis and otitis media

because of a failure of the mucociliary defense system in the nasal passages and possibly in the eustachian tube.

Cilia paucity in Cby$^{-/-}$ mice

Defects in MCT may be caused either by abnormal cilia structure or by reduced numbers of cilia. To examine cilia structure, we analyzed nasopharyngeal cilia by transmission EM (TEM).
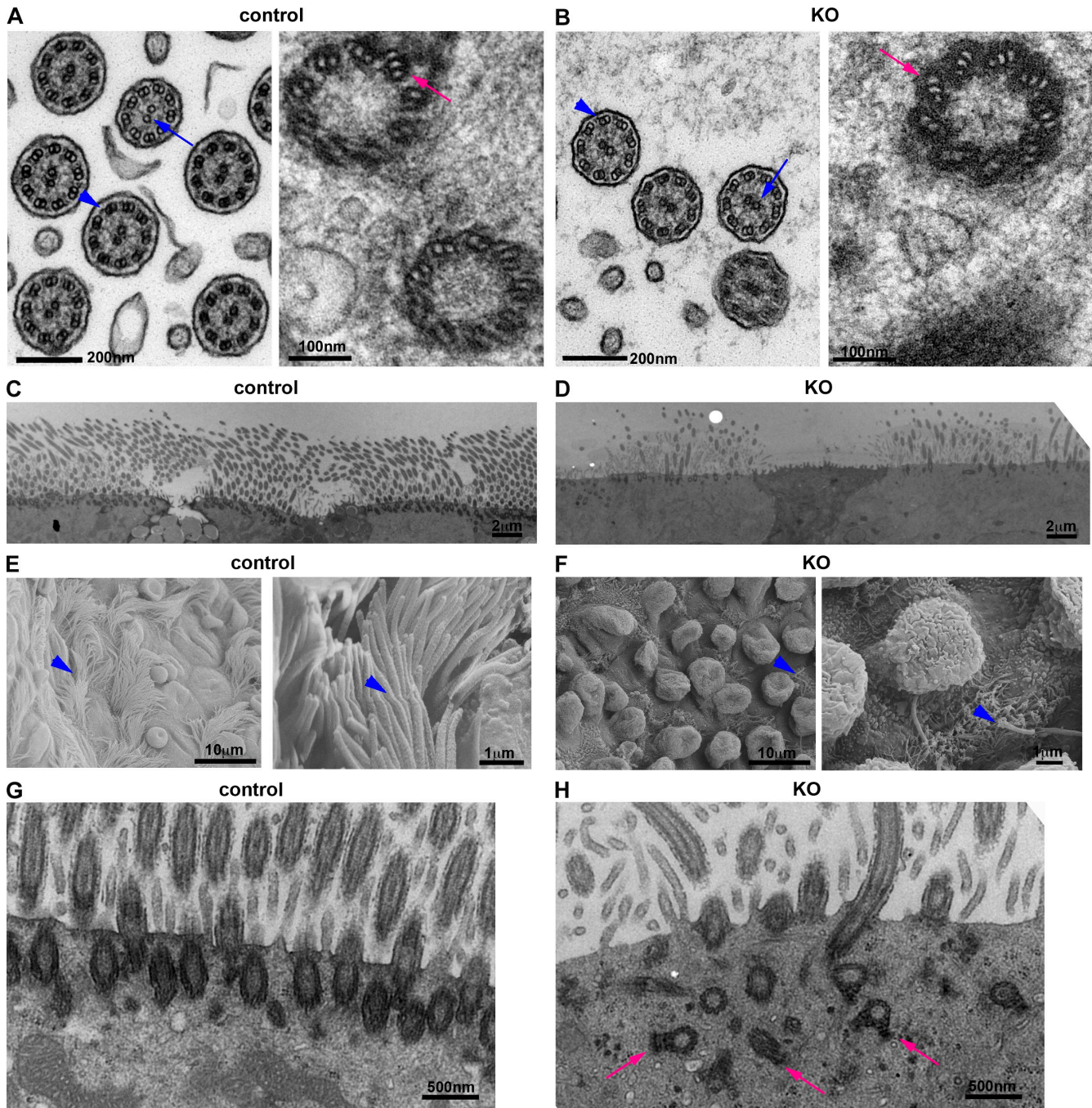
Figure 3. **Ultrastructure of airway cilia in $Cby^{-/-}$ mice.** (A and B) TEM analysis of cross sections of nasopharyngeal motile cilia and basal bodies in 4-wk-old $Cby^{+/+}$ and $Cby^{-/-}$ mice. Blue arrows and arrowheads indicate central microtubule pairs and outer dynein arms, respectively. Pink arrows point to microtubule triplets in the basal body. (C and D) TEM analysis of nasopharyngeal motile cilia in adult $Cby^{+/+}$ and $Cby^{-/-}$ mice. (E and F) Scanning EM analysis of ciliated cells in the large proximal airways of adult $Cby^{+/+}$ and $Cby^{-/-}$ mice. Blue arrowheads indicate ciliated cells. In addition to cilia, the apical surface of ciliated cells contains microvilli of variable number and length. (G and H) TEM analysis of nasopharyngeal basal bodies from adult $Cby^{+/+}$ and $Cby^{-/-}$ mice. Pink arrows highlight abnormally localized basal bodies. KO, knockout.

Cilia from $Cby^{-/-}$ mice exhibit apparently normal ciliary ultrastructure with a 9 + 2 microtubular arrangement and the presence of outer dynein arms (Fig. 3, A and B). Basal bodies in $Cby^{-/-}$ mice also show normal nine-triplet structure (Fig. 3, A and B). Similarly, we did not detect any apparent defects in the structure of bronchial cilia from $Cby^{-/-}$ mice (Fig. S2, A and B). In the course of our TEM experiments, we noticed that $Cby^{-/-}$ mice have an abnormally low abundance of cilia in their

nasopharynx (Fig. 3, compare C with D). A marked paucity of cilia was also observed upon analysis of $Cby^{-/-}$ nasopharyngeal tissue at P0 (Fig. S2, C and D), ruling out the possibility that loss of cilia is secondary to chronic inflammation. To verify our observation, we performed scanning EM analysis of proximal lung airways from adult $Cby^{-/-}$ and $Cby^{+/+}$ mice. We found that the number of cilia is dramatically decreased in the $Cby^{-/-}$ tissue when compared with that from $Cby^{+/+}$ controls (Fig. 3, E and F).

nasal epithelium

WT: ac-tubulin (A) | Cby (B) | overlay (C)

KO: ac-tubulin (D) | Cby (E) | overlay (F)

MDCK2 cells

ac-tubulin (G) | Cby (H) | overlay (I)

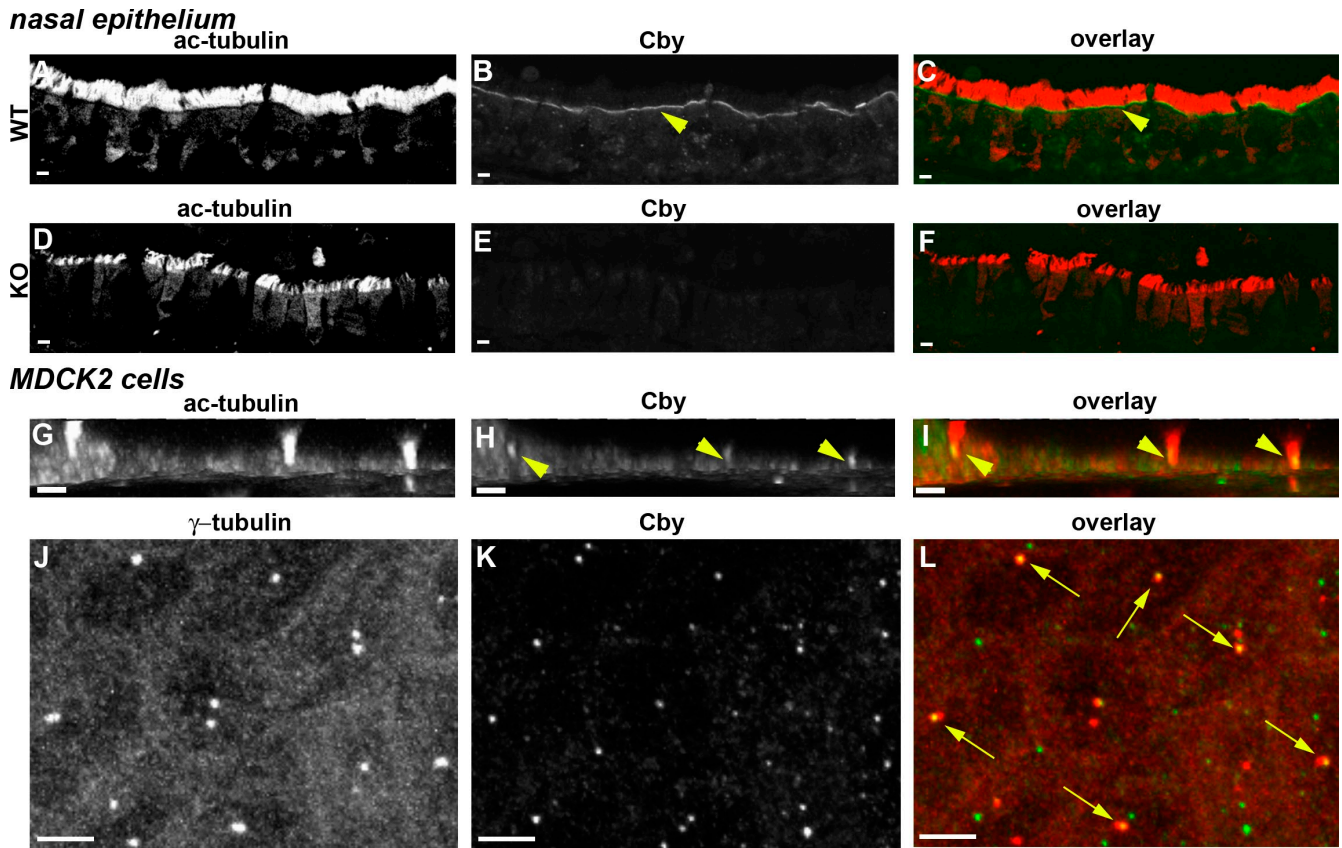γ–tubulin (J) | Cby (K) | overlay (L)

Figure 4. **Cellular localization of Cby protein.** (A–F) Nasal epithelial sections from $Cby^{+/+}$ (A–C) and $Cby^{-/-}$ (D–F) adult mice were double stained with antibodies against acetylated α-tubulin (ac-tubulin; A and D) and Cby (B and E), and the merged images of acetylated α-tubulin (red) and Cby (green) are shown (C and F). (G–I) Ciliated MDCK2 cells were doubly immunostained with acetylated α-tubulin (G) and Cby (H) antibodies, and the merged image of acetylated α-tubulin (red) and Cby (green) is shown (I). (J–L) Ciliated MDCK2 cells were double stained with γ-tubulin (J) and Cby (K), and the merged image of γ-tubulin (red) and Cby (green) is shown (L). Arrows show colocalization of Cby with γ-tubulin. (B, C, H, and I) Arrowheads point out Cby staining at the base of the cilia. Bars: (A–F) 6 µm; (G–I) 1 µm; (J–L) 5 µm.

Collectively, we conclude that loss of Cby results in a paucity of cilia in respiratory tracts, which most likely accounts for the lack of MCT activity in $Cby^{-/-}$ mice.

Based on these data, we hypothesized that the ciliary defects in $Cby^{-/-}$ mice might be caused by altered docking or transport of basal bodies to the apical membrane. Through detailed EM analysis, we found that a significant number of basal bodies failed to position apically and dock at the plasma membrane in $Cby^{-/-}$ nasal ciliated cells (Fig. 3, G and H). This is not attributable to a general loss of apical–basal polarity in these cells because the apical marker ZO1 and actin filaments as well as the basolateral marker epithelial cadherin remained unaffected in $Cby^{-/-}$ mice (Fig. S3, M–R). As cilia extend from basal bodies, compromised basal body docking may explain, at least in part, the defective ciliogenesis in $Cby^{-/-}$ mice.

Cby protein is localized at the ciliary base

Given the involvement of *Cby* in cilia pathology, we asked whether Cby protein is localized in a manner consistent with this pathology. Double immunostaining with an antibody against acetylated α-tubulin (cilia marker) revealed that Cby is localized at the ciliary base in multiciliated cells of the adult $Cby^{+/+}$ nasal epithelium (Fig. 4, A–C), whereas no Cby staining was detected in the $Cby^{-/-}$ tissue (Fig. 4, D–F). In agreement with

this, Cby protein is expressed in ciliated cells in the developing lung airways and esophagus at E18.5 (Fig. S2, E–G). Additionally, endogenous Cby was detected at the base of primary cilia in cultured MDCK2 cells (Fig. 4, G–I). We also noted that Cby colocalizes with the centrosomal marker γ-tubulin (Fig. 4, J–L). Several ciliopathy-associated proteins have been shown to localize to both centrosomes and basal bodies, including CEP290, which is involved in Joubert syndrome (Valente et al., 2006), and ALMS1, which is mutated in Alström syndrome (Li et al., 2007). Cby localization at the base of the cilia further supports our notion that Cby is directly involved in ciliogenesis.

Wnt–β-catenin signaling activity in $Cby^{-/-}$ mice

Cby acts as an antagonist of Wnt–β-catenin signaling in mammalian cultured cells and *Drosophila melanogaster* embryos (Takemaru et al., 2003). Thus, we evaluated the status of β-catenin–dependent transcription in nasal epithelia from $Cby^{-/-}$ mice and age-matched controls using quantitative PCR for the direct β-catenin targets *Axin2* and *CyclinD1*. We observed a consistent increase in the expression of these genes in the $Cby^{-/-}$ tissue (Fig. 5 A). Similar results were obtained for primary mouse embryonic fibroblasts (PMEFs) derived from $Cby^{-/-}$ and $Cby^{+/+}$ embryos (Fig. 5 B). These data are consistent with Cby
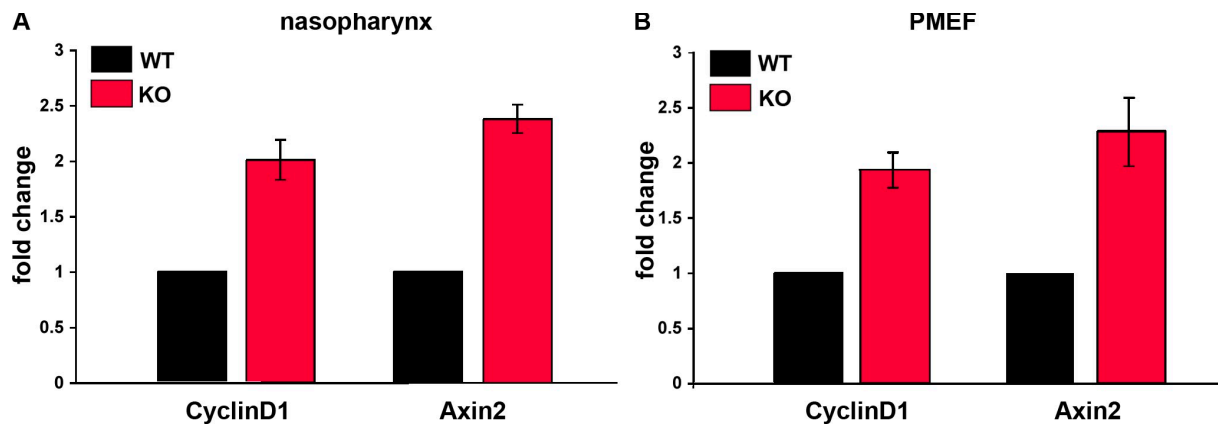
Figure 5. Effect of *Cby* inactivation on Wnt–β-catenin signaling. (A and B) Real-time PCR analysis was performed for expression levels of β-catenin target genes in the nasal epithelium from adult mice (*n* = 4 for each genotype; A) or PMEFs (*n* = 6 for each genotype; B). Wild-type (WT) values were set as 1. Data are represented as means ± SEM. KO, knockout.

being a β-catenin antagonist (Takemaru et al., 2003) and raise the question of whether *Cby*^{−/−} mice display changes in the localization of Wnt–β-catenin pathway components such as adenomatosis polyposis coli, β-catenin, and Dishevelled, which have been shown to localize to the ciliary base (Gerdes et al., 2007; Corbit et al., 2008; Park et al., 2008). Therefore, we analyzed the localization of β-catenin and Dvl1 in nasal ciliated cells from *Cby*^{−/−} mice and littermate controls. Lateral membranous β-catenin and apical Dvl1 localization remained unchanged in the absence of Cby (Fig. S3, A–L). Based on these results, it is not clear whether the ciliary phenotypes of *Cby*^{−/−} mice are related to the modest elevation of Wnt–β-catenin target genes in these mice. These and other questions that seek to link the mechanisms of Wnt signaling to discrete subcellular compartments and structures await further research.

Similarities to disease phenotypes

The airway phenotypes of *Cby*^{−/−} mice bear strong similarities to those of human PCD patients. PCD is frequently associated with mutations in genes encoding dyneins, including *DNAH1* and *DNAH5* (Pennarun et al., 1999; Olbrich et al., 2002). Our quantitative PCR analysis demonstrated that inactivation of *Cby* did not significantly affect levels of *Dnah1* and *Dnah5* transcripts in nasal epithelial tissue (unpublished data).

The presence of sinusitis and otitis media and an inability to clear bacteria from the sinuses upon intranasal infection underlie similarities between the phenotypic defects found in *Cby*^{−/−} mice and in human patients with PCD. This is especially evident when *Cby*^{−/−} mice are exposed to bacterial challenge, exacerbating the already inflamed state of their upper airway. About half of PCD patients have laterality defects and many are subfertile (Meeks and Bush, 2000; Noone et al., 2004). To date, we have not observed left–right patterning defects such as situs inversus in *Cby*^{−/−} mice, suggesting that Cby is not essential for proper structure and function of motile 9 + 0 cilia in the embryonic node. We noticed partially penetrant infertility in *Cby*^{−/−} males (unpublished data). All of these observations signify similarities between phenotypes of *Cby*^{−/−} mice and human patients with PCD.

Current animal models of PCD with respiratory pathology have abnormal ciliary structure (Ibanez-Tallon et al., 2002;

Kobayashi et al., 2002). Although the majority of PCD patients also show defects in airway cilia structure, ∼10% of atypical PCD cases show cilia with normal axoneme structure (Livraghi and Randell, 2007; Zariwala et al., 2007). This allows us to speculate that a subset of PCD may be caused by mutations in the *Cby* gene. Thus, *Cby*^{−/−} mice might serve as a model for atypical cases of PCD. Given that the existing mouse models of PCD exhibit very high incidence of hydrocephalus and perinatal lethality, surviving *Cby*^{−/−} mice may also be useful as an animal model for long-term studies of chronic upper airway infections (Livraghi and Randell, 2007).

Materials and methods

Northern blotting
Northern blots were purchased from OriGene and hybridized with a ^{32}P-labeled full-length mouse *Cby* cDNA probe. The probe was synthesized by random priming using the DECAprime II kit (Applied Biosystems).

Generation of *Cby*^{−/−} mice
A bacterial artificial chromosome (BAC) clone containing the *Cby* gene was isolated from the mouse 129 BAC library (Invitrogen). The BAC clone was characterized by restriction mapping and sequencing. An upstream 4.1-kb BamHI–StuI fragment and a downstream 4.1-kb XbaI–SmaI fragment were subcloned into PGKneoF2L2DTA targeting vector (a gift from P. Soriano, Fred Hutchinson Cancer Research Center, Seattle, WA) on either side of the neomycin resistance cassette to replace the whole *Cby* coding sequence. The linearized construct was electroporated into R1 embryonic stem cells, and transfectants resistant to G418 were screened for homologous recombination by Southern blot analysis. Of the 17 neomycin-resistant clones analyzed, 5 (29%) contained the correctly targeted *Cby* allele. Three independent targeted cell lines were separately injected into blastocysts by the transgenic mouse facility at the University of Washington. Chimeric males were crossed with female C57BL/6 mice, and germline transmission was detected by the presence of agouti-colored offspring and further confirmed by Southern blot analysis (Fig. S1 B). All three embryonic stem cell clones successfully underwent germline transmission, and all three mouse lines showed identical phenotypes. Mice characterized in this paper were backcrossed to C57BL/6 mice at least five times (≥N5 generation). Genotyping was performed by PCR (Fig. S1 C); the primer sequences used for genotyping were P1, 5′-TGCCATTACACGAGAC-TAGACAG-3′; P2, 5′-AGACACCAGTGTCAAGAGGTGAG-3′; and P3, 5′-CTTTCTAGAGAATAGGAACTTCGG-3′.

Mice were fed irradiated Picolab Rodent Diet 20 (PMI Nutrition International) and reverse osmosis water. All supplies entering animal rooms were autoclaved, and rooms were maintained at 70–74°F and 45–55% humidity, with 28 air changes/h and a 12-h light/12-h dark cycle. All

animal procedures were approved by the University of Washington Animal Care and Use Committee.

In situ hybridization
Whole mount in situ hybridizations were performed as previously described (Cygan et al., 1997).

Histological analysis
Mice were euthanized by CO_2 asphyxiation in accordance with the University of Washington Animal Care and Use Committee procedures. Complete necropsies were performed, and tissues were dissected and immersion fixed in 10% neutral buffered formalin. Skulls were decalcified in Cal-rite (Richard-Allan Scientific). Samples were then processed routinely by paraffin embedding. All tissues were initially stained with hematoxylin and eosin (H&E) and examined histologically, and selected sections were also stained with giemsa or periodic acid Schiff.

TEM
For cross section TEM analysis of the main stem bronchus, tissue was removed, fixed in 2% glutaraldehyde/2% formaldehyde in 0.1 M Sorenson's buffer, and postfixed in 1% osmium tetroxide in Sorenson's buffer. Samples were then embedded in epon resin (Poly/Bed812; Polysciences), and 90-nm sections were cut, stained with 7% uranyl acetate/0.3% lead citrate, and viewed using an electron microscope (EM900; Carl Zeiss, Inc.). For cross section TEM analysis of the nasopharynx, tissue was removed, fixed in 2.5% glutaraldehyde/2% formaldehyde in 0.1 M cacodylate buffer, and postfixed in 1% osmium tetroxide in cacodylate buffer. Samples were then embedded in epon resin (Poly/Bed812), and 70–90-nm sections were cut, stained with 6% aqueous uranyl acetate and Reynold's lead citrate, and viewed using an electron microscope (model 1230; JEOL) with a 2,000 × 2,000–pixel charge-coupled device camera (Ultrascan 1000; Gatan). Images were adjusted for brightness and contrast using Photoshop (Adobe).

Scanning EM
Adult lungs were inflation fixed with 4% PFA, and proximal lung tissue was removed. The tissue was then dehydrated using a graded ethanol series to 100% and transferred to 100% hexamethyldisilazane (HMDS; Electron Microscopy Sciences) through a graded series of ethanol-HMDS mixtures. The specimens were air dried, mounted on scanning EM stubs, and sputter coated with gold before examination with a scanning electron microscope (LEO1550; Carl Zeiss, Inc.) at 10 kV using a back scatter detector (Robinson). Images were processed using Photoshop.

Bacterial challenge
An overnight culture of PAO-SC11, a mutant of PAO1 *P. aeruginosa* (Chugani and Greenberg, 2007), was diluted 1:10 in Luria broth (LB) and grown for another 1 h to an OD of ~1.0 at 600 nm on the morning of infection. The bacteria were harvested by centrifugation, resuspended in PBS with 10 mM $MgCl_2$, and diluted to the desired concentration. Actual counts were determined by serial dilution and plating on LB agar plates. Mice were anesthetized with 130 mg/kg ketamine plus 9 mg/kg xylazine and infected intranasally with 30 µl PAO-SC11. A group of control mice was euthanized immediately after infection to determine actual deposition in the lungs. Lungs were homogenized in PBS containing 10 mM $MgCl_2$ and 0.05% Triton X-100, and CFU analysis was performed by serial dilution and plating on LB and *P. aeruginosa* isolation agar plates (BD). At 72 h after infection, $Cby^{-/-}$ and control mice were euthanized, lungs were collected for CFU analysis, and sinuses were fixed and subjected to the aforementioned histological analysis. Prism software (GraphPad Software, Inc.) was used to analyze CFU results using a one-way analysis of variance test.

Tracheal electrophysiology
Mice were euthanized by CO_2 asphyxiation, and the trachea was isolated, split longitudinally, removed from the mouse, and positioned on the 0.025-cm^2 aperture of an Ussing chamber as previously described (Grubb et al., 1994). The tissue was bathed bilaterally in Krebs Ringer bicarbonate buffer and studied under short circuit current conditions (Grubb et al., 1994). To assess the magnitude of electrogenic Na^+ absorption, 10^{-4} M amiloride was added apically after a 30-min equilibration period. 5 min later, 10^{-4} M UTP (induces Cl^- secretion via the Ca^{2+}-activated Cl^- conductance) was added followed by 10^{-5} M apical forskolin (induces an increase in Cl^- secretion by increasing cAMP levels). All drugs were purchased from Sigma-Aldrich.

MCT measurements
Mice were euthanized by CO_2 inhalation, and the lower jaw was removed, exposing the hard and soft palate. An incision was made through the skin and fascia over the most caudal palatine fold. The skin and fascia were then carefully removed from the soft palate by peeling the tissue caudally using fine forceps. Once the skin and fascia were stripped from the soft palate, the very thin ventral wall of the nasopharyngeal meatus became evident, and the beating cilia on the apical side of the membrane were seen clearing debris caudally. Next, water-equilibrated mineral oil was applied to the membrane to prevent desiccation. As the cilia are on the opposite side of the membrane (and the nasopharyngeal meatus is not actually opened), the mineral oil did not contact the cilia. For image acquisition, the preparation was placed under a dissecting microscope (Om3300/V10-7X-10X stereo; Omano). A video camera (CCD72; MTI) was mounted on the scope and interfaced with a VHS recorder and monitor. Before MCT was recorded, a slide micrometer was placed on the stage of the dissecting scope, and the image was recorded. When the data were reduced, the video monitor was calibrated for distance using the recorded image of the slide micrometer. Once the video was recorded, MCT was determined by playing the video back and determining the time it took endogenously secreted mucus and other inhaled debris present in the nasal cavity before euthanasia to traverse the calibrated distance (usually an in vivo distance of 0.5–1 mm) on the monitor screen. Time was recorded with a stopwatch (accurate to 0.01 s), and MCT was calculated as millimeters per minute.

RNA extraction and real-time RT-PCR
Total RNA was purified from PMEFs and from nasopharyngeal epithelia using the RNeasy Mini kit (QIAGEN), with DNase digestion performed with the RNase-free DNase set (QIAGEN). First-strand cDNA synthesis and PCR amplification were performed with 100 ng of RNA template using the iScript One-Step RT-PCR kit with SYBR Green (Bio-Rad Laboratories) and the MiniOpticon real-time PCR detection system (Bio-Rad Laboratories) according to the manufacturer's instructions. The primer pairs used were *CyclinD1* (5′-TGTTCGTGGCCTCTAAGATGAAG-3′ and 5′-AGGTTC-CACTTGAGCTTGTTCAC-3′), *Axin2* (5′-CTCCCCACCTTGAATGAAGA-3′ and 5′-ACATAGCCGGAACCTACGTG-3′), and *ARBP* (5′-TGTTTGACAAC-GGCAGCATTT-3′ and 5′-CCGAGGCAACAGTTTGGGTA-3′). The level of transcripts for *ARBP* was used as an internal standard. Samples were analyzed in triplicate.

Immunostaining
For immunofluorescence staining, MDCK2 cells were grown to confluency and then serum starved for 48 h to induce ciliation. Cells were fixed either in 4% PFA or in ice-cold methanol, washed in PBS, permeabilized with 0.1% Triton X-100 in PBS, and incubated with primary and secondary antibodies. The nasal epithelium was removed and processed as for routine histological analysis, and sections were incubated with primary and secondary antibodies. Stained sections were mounted with ProLong Gold antifade reagent with DAPI (Invitrogen). Images were acquired at room temperature using a confocal microscope (SP1/MP; Leica) equipped with 40× Plan-Apochromat NA 1.25 oil immersion, 100× Plan-Apochromat NA 1.40 oil immersion, and 63× Plan-Apochromat NA 1.20 water immersion objectives and confocal software (Leica). Images were analyzed and three-dimensionally visualized using Imaris software (Bitplane) and assembled in figure format in Photoshop. Primary antibodies used were anti–acetylated α-tubulin (1:10,000; Sigma-Aldrich), anti–γ-tubulin (1:400; Sigma-Aldrich), Dvl1 (1:500; Santa Cruz Biotechnology, Inc.), ZO1 (1:500; Invitrogen), epithelial cadherin (1:500; BD), and 15B8 β-catenin (1:500; Sigma-Aldrich). We also used Alexa Fluor 488 phalloidin (1:100; Invitrogen) to visualize the actin cytoskeleton. Rabbit anti-Cby polyclonal antibody was raised against the N-terminal portion of mouse Cby, purified by antigen affinity chromatography at Covance, and used at a 1:500 dilution. Alexa Fluor 488 and Alexa Fluor 568 secondary antibodies were purchased from Invitrogen.

Online supplemental material
Fig. S1 shows gene targeting at the mouse *Cby* locus. Fig. S2 shows the axonemal structure of adult bronchial cilia, a paucity of nasal cilia in newborn mice, and Cby expression in embryonic lung and esophageal epithelia at E18.5. Fig. S3 shows immunostaining for β-catenin, Dvl1, and apical–basal markers in the adult nasal epithelium. Videos 1 and 2 compare MCT in the nasopharyngeal cavities of adult $Cby^{+/+}$ and $Cby^{-/-}$ mice. Online supplemental material is available at http://www.jcb.org/cgi/content/full/jcb.200809144/DC1.

References

Badano, J.L., N. Mitsuma, P.L. Beales, and N. Katsanis. 2006. The ciliopathies: an emerging class of human genetic disorders. *Annu. Rev. Genomics Hum. Genet.* 7:125–148.

Bush, A., and T. Ferkol. 2006. Movement: the emerging genetics of primary ciliary dyskinesia. *Am. J. Respir. Crit. Care Med.* 174:109–110.

Christensen, S.T., L.B. Pedersen, L. Schneider, and P. Satir. 2007. Sensory cilia and integration of signal transduction in human health and disease. *Traffic*. 8:97–109.

Chugani, S., and E.P. Greenberg. 2007. The influence of human respiratory epithelia on *Pseudomonas aeruginosa* gene expression. *Microb. Pathog.* 42:29–35.

Cohen, N.A. 2006. Sinonasal mucociliary clearance in health and disease. *Ann. Otol. Rhinol. Laryngol. Suppl.* 196:20–26.

Corbit, K.C., A.E. Shyer, W.E. Dowdle, J. Gaulden, V. Singla, and J.F. Reiter. 2008. Kif3a constrains beta-catenin-dependent Wnt signalling through dual ciliary and non-ciliary mechanisms. *Nat. Cell Biol.* 10:70–76.

Coren, M.E., M. Meeks, I. Morrison, R.M. Buchdahl, and A. Bush. 2002. Primary ciliary dyskinesia: age at diagnosis and symptom history. *Acta Paediatr.* 91:667–669.

Cygan, J.A., R.L. Johnson, and A.P. McMahon. 1997. Novel regulatory interactions revealed by studies of murine limb pattern in Wnt-7a and En-1 mutants. *Development*. 124:5021–5032.

Davis, E.E., M. Brueckner, and N. Katsanis. 2006. The emerging complexity of the vertebrate cilium: new functional roles for an ancient organelle. *Dev. Cell*. 11:9–19.

Eley, L., L.M. Yates, and J.A. Goodship. 2005. Cilia and disease. *Curr. Opin. Genet. Dev.* 15:308–314.

Gerdes, J.M., Y. Liu, N.A. Zaghloul, C.C. Leitch, S.S. Lawson, M. Kato, P.A. Beachy, P.L. Beales, G.N. DeMartino, S. Fisher, et al. 2007. Disruption of the basal body compromises proteasomal function and perturbs intracellular Wnt response. *Nat. Genet.* 39:1350–1360.

Gibson, R.L., J.L. Burns, and B.W. Ramsey. 2003. Pathophysiology and management of pulmonary infections in cystic fibrosis. *Am. J. Respir. Crit. Care Med.* 168:918–951.

Grubb, B.R., A.M. Paradiso, and R.C. Boucher. 1994. Anomalies in ion transport in CF mouse tracheal epithelium. *Am. J. Physiol.* 267:C293–C300.

Hidaka, S., V. Konecke, L. Osten, and R. Witzgall. 2004. PIGEA-14, a novel coiled-coil protein affecting the intracellular distribution of polycystin-2. *J. Biol. Chem.* 279:35009–35016.

Ibanez-Tallon, I., S. Gorokhova, and N. Heintz. 2002. Loss of function of axonemal dynein Mdnah5 causes primary ciliary dyskinesia and hydrocephalus. *Hum. Mol. Genet.* 11:715–721.

Kobayashi, Y., M. Watanabe, Y. Okada, H. Sawa, H. Takai, M. Nakanishi, Y. Kawase, H. Suzuki, K. Nagashima, K. Ikeda, and N. Motoyama. 2002. Hydrocephalus, situs inversus, chronic sinusitis, and male infertility in DNA polymerase lambda-deficient mice: possible implication for the pathogenesis of immotile cilia syndrome. *Mol. Cell. Biol.* 22:2769–2776.

Kramer-Zucker, A.G., F. Olale, C.J. Haycraft, B.K. Yoder, A.F. Schier, and I.A. Drummond. 2005. Cilia-driven fluid flow in the zebrafish pronephros, brain and Kupffer's vesicle is required for normal organogenesis. *Development*. 132:1907–1921.

Li, F.Q., A. Mofunanya, K. Harris, and K. Takemaru. 2008. Chibby cooperates with 14-3-3 to regulate β-catenin subcellular distribution and signaling activity. *J. Cell Biol.* 181:1141–1154.

Li, G., R. Vega, K. Nelms, N. Gekakis, C. Goodnow, P. McNamara, H. Wu, N.A. Hong, and R. Glynne. 2007. A role for Alström syndrome protein, alms1, in kidney ciliogenesis and cellular quiescence. *PLoS Genet.* 3:e8.

Livraghi, A., and S.H. Randell. 2007. Cystic fibrosis and other respiratory diseases of impaired mucus clearance. *Toxicol. Pathol.* 35:116–129.

Meeks, M., and A. Bush. 2000. Primary ciliary dyskinesia (PCD). *Pediatr. Pulmonol.* 29:307–316.

Nauli, S.M., F.J. Alenghat, Y. Luo, E. Williams, P. Vassilev, X. Li, A.E. Elia, W. Lu, E.M. Brown, S.J. Quinn, et al. 2003. Polycystins 1 and 2 mediate mechanosensation in the primary cilium of kidney cells. *Nat. Genet.* 33:129–137.

Noone, P.G., M.W. Leigh, A. Sannuti, S.L. Minnix, J.L. Carson, M. Hazucha, M.A. Zariwala, and M.R. Knowles. 2004. Primary ciliary dyskinesia: diagnostic and phenotypic features. *Am. J. Respir. Crit. Care Med.* 169:459–467.

Olbrich, H., K. Haffner, A. Kispert, A. Volkel, A. Volz, G. Sasmaz, R. Reinhardt, S. Hennig, H. Lehrach, N. Konietzko, et al. 2002. Mutations in DNAH5 cause primary ciliary dyskinesia and randomization of left-right asymmetry. *Nat. Genet.* 30:143–144.

Ong, A.C., and B. Wagner. 2005. Detection of proximal tubular motile cilia in a patient with renal sarcoidosis associated with hypercalcemia. *Am. J. Kidney Dis.* 45:1096–1099.

Park, T.J., B.J. Mitchell, P.B. Abitua, C. Kintner, and J.B. Wallingford. 2008. Dishevelled controls apical docking and planar polarization of basal bodies in ciliated epithelial cells. *Nat. Genet.* 40:871–879.

Pazour, G.J., N. Agrin, J. Leszyk, and G.B. Witman. 2005. Proteomic analysis of a eukaryotic cilium. *J. Cell Biol.* 170:103–113.

Pennarun, G., E. Escudier, C. Chapelin, A.M. Bridoux, V. Cacheux, G. Roger, A. Clement, M. Goossens, S. Amselem, and B. Duriez. 1999. Loss-of-function mutations in a human gene related to *Chlamydomonas reinhardtii* dynein IC78 result in primary ciliary dyskinesia. *Am. J. Hum. Genet.* 65:1508–1519.

Salathe, M. 2007. Regulation of mammalian ciliary beating. *Annu. Rev. Physiol.* 69:401–422.

Singla, V., and J.F. Reiter. 2006. The primary cilium as the cell's antenna: signaling at a sensory organelle. *Science*. 313:629–633.

Takemaru, K., S. Yamaguchi, Y.S. Lee, Y. Zhang, R.W. Carthew, and R.T. Moon. 2003. Chibby, a nuclear beta-catenin-associated antagonist of the Wnt/Wingless pathway. *Nature*. 422:905–909.

Teilmann, S.C., C.A. Clement, J. Thorup, A.G. Byskov, and S.T. Christensen. 2006. Expression and localization of the progesterone receptor in mouse and human reproductive organs. *J. Endocrinol.* 191:525–535.

Valente, E.M., J.L. Silhavy, F. Brancati, G. Barrano, S.R. Krishnaswami, M. Castori, M.A. Lancaster, E. Boltshauser, L. Boccone, L. Al-Gazali, et al. 2006. Mutations in CEP290, which encodes a centrosomal protein, cause pleiotropic forms of Joubert syndrome. *Nat. Genet.* 38:623–625.

Zariwala, M.A., M.R. Knowles, and H. Omran. 2007. Genetic defects in ciliary structure and function. *Annu. Rev. Physiol.* 69:423–450.